

# Wavelet-based extraction of building features from airborne laser scanner data

T. Thuy Vu, Mitsuharu Tokunaga, and Fumio Yamazaki

**Abstract.** A new approach based on wavelet analysis to detect buildings in a dense urban area from airborne laser scanner data is presented in this paper. Without the spectral reflectance from the buildings, their detection from the laser cloud points is mainly based on the discrimination of the building's elevation and its surroundings. This detection becomes more challenging in a dense urban area, which contains skyscrapers, interspersed with a myriad of low and small as well as large houses along with crowded outdoor human activities. Integration of the object's size and its elevation could mitigate the difficulty of detection. Wavelet analysis was proposed and adopted to build up the framework for size-based detection. The study focused on the detection of buildings and the generation of a three-dimensional (3D) building database. The extractable information from the aerial photographs is optional. The proposed approach was tested in Shinjuku-ku, Tokyo, Japan, and the result has successfully matched with the existing two-dimensional (2D) vector data. Wavelet-based multi-resolution has proved an appropriate approach in eliminating the unnecessary features surrounding buildings and in extracting the buildings.

**Résumé.** On présente une nouvelle approche basée sur l'analyse en ondelettes pour la détection des bâtiments dans une zone urbaine dense à l'aide des données d'un balayeur laser aéroporté. Sans l'aide de la réflectance spectrale émise à partir des bâtiments, la détection des bâtiments à l'aide d'un nuage de points laser repose principalement sur la discrimination des hauteurs des bâtiments par rapport à l'environnement immédiat. La détection devient plus difficile dans une zone urbaine dense présentant un assortiment de gratte ciel, où sont intercalés une multitude de maisons basses et petites de même que des maisons plus grandes, accompagnées d'activités humaines extérieures intensives. L'intégration de la dimension des objets et de leur hauteur peut aider à temporiser la difficulté de détection. L'analyse en ondelettes est proposée et adoptée pour l'élaboration d'un cadre pour la détection basée sur la dimension. L'étude s'est intéressée principalement à la détection des bâtiments et à la génération d'une base de données 3D des bâtiments. L'information que l'on peut extraire des photographies aériennes est optionnelle. L'approche proposée a été testée dans la zone de Shinjuku-ku, Tokyo, au Japon, et les résultats concordaient avec les données vectorielles 2D existantes. L'analyse multirésolution en ondelettes s'est révélée une approche utile pour l'élimination des caractéristiques non essentielles autour des bâtiments et pour l'extraction des bâtiments.

[Traduit par la Rédaction]

## Introduction

Airborne laser scanner data is an integrated system consisting of global positioning system (GPS), inertial navigation system (INS), and laser scanner. It sends the laser pulse, receives the laser hit on the earth's surface, and has been considered as a highly accurate tool for topographic mapping (Wehr and Lohr, 1999). A variety of algorithms for building extractions have been developed. Maas and Vosselman (1999) and Vosselman (1999) developed algorithms for reconstruction of buildings from the laser scanner data only. To obtain reliable results, the laser scanner data should be of high density with 5–7 points/m<sup>2</sup>. The limitation of the laser scanner system is that it provides only coordinates (Axelsson, 1999). Through a higher density of laser scanner data, more information about the shapes of buildings can be obtained. However, the density of laser points varies from system to system. The other category of developed algorithms is detection with the extractable information from aerial photograph (Haala, 1994; Haala and Brenner, 1999). This kind of algorithm utilizes the information extracted from aerial photograph and helps refine the shapes of the objects.

In principle, any proposed algorithm should be able to work across different density values of laser scanner data. Furthermore, it should be able to work with or without the availability of aerial photographs or high-resolution satellite imagery. However, the distribution of objects in a dense urban area is very complicated. It creates difficulty in detecting objects from both aerial photographs and airborne laser scanner data. Fortunately, the buildings in an urban area appear considerably larger than other objects, such as trees or cars. Including aspects of building size may improve the

---

Received 19 November 2002. Accepted 12 May 2003.

**T. Thuy Vu.**<sup>1</sup> Space Technology Applications and Research Program, Asian Institute of Technology, 12120, Thailand.

**M. Tokunaga.** Environmental System Engineering, Kanazawa Institute of Technology, Ishikawa 921-8501, Japan.

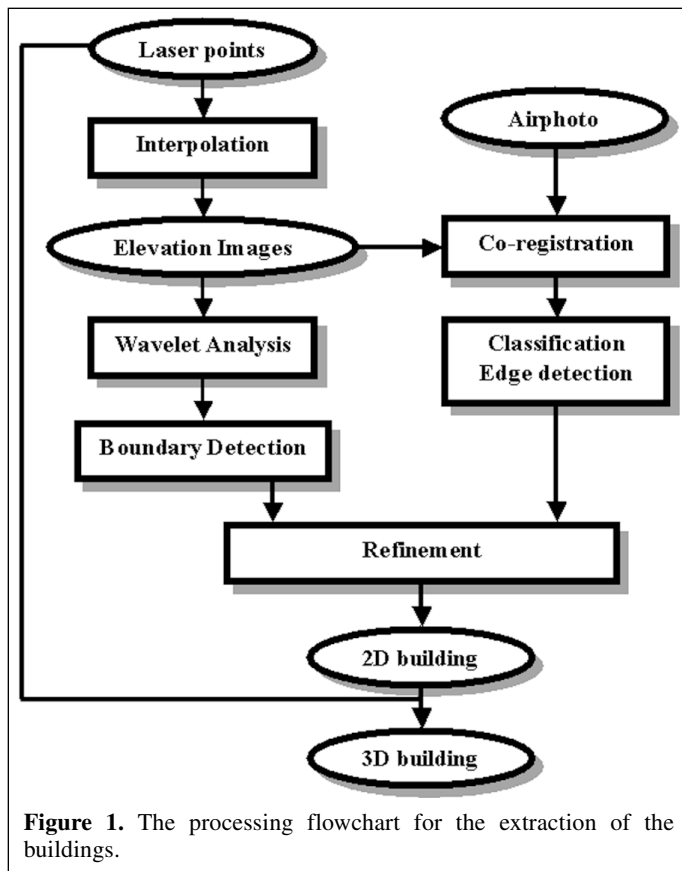
**F. Yamazaki.** Institute of Industrial Science, University of Tokyo, Tokyo, Japan.

<sup>1</sup>Corresponding author. Present address: Disaster Information System Team, Earthquake Disaster Mitigation Research Center (EDM), National Institute for Earth Science and Disaster Prevention (NIED), 1-5-2 Kaigandori, Wakinohama, Chuo-ku, Kobe 651-0073, Japan (e-mail: thuyvu@edm.bosai.go.jp).

performance of detection algorithm. Analysis of objects in the image or the cloud points at different resolutions has been proved as an excellent approach to detect and extract the target objects (Lega et al., 1995; Starck and Murtagh, 1994). The key point is that the objects appear only at a certain range of scale or resolution. Wavelet-based multi-resolution analysis has been adopted as a powerful analysis tool by researchers and engineers of different fields. With a beginning in the early 20th century by Alfred Haar (Daubechies, 1992), the mathematical foundation of wavelet analysis is now firmly established (Daubechies, 1992). The fundamental idea of wavelet is to analyze the signal according to scale or resolution. In this study, wavelet-based algorithm is introduced for the detection of objects from the airborne laser scanner data. This study also evaluates the performance of the proposed approach on low-density laser data of about 0.2 points/m<sup>2</sup>.

## Methodology

The scheme for the extraction of the buildings is part of the new proposed approach for the classification of laser points and extraction of features. It is based on wavelet and is referred to as “ALSwave” in this paper. **Figure 1** illustrates the complete processing for the extraction of the buildings. The step-by-step processing of the proposed approach is described in the following sections.



## Interpolation

To maintain the surface discontinuity typifying an urban area, the planar interpolation method on the triangulated irregular network (TIN) was preferred. The higher degree of interpolation will smooth and, therefore, eliminate the sharp edges of the buildings. It is noted that there might be shadow, i.e., no reflected laser points, owing to skyscrapers located near the edge of the flight strip. This shadow causes the displacement of the detected edges of the buildings from the most potential position. Based on the assumption that the surface is flat in the shadow, the adjustment could be carried out by adding pseudo points as illustrated in the following steps.

### Selection of region of interest (ROI)

A number of ROIs were selected along the edges of the buildings, which could be located from the above generated TIN. These ROIs were statistically investigated to set up the threshold values for the next processing steps.  $S$  is the set of selected ROIs, i.e.,  $S = S_k, k = 1, 2, \dots, K$ ;  $OP_k$  and  $P_k$  is the building laser point set and ground laser point set of  $S_k$ , i.e.,  $OP_k = OP_{ki}, i = 1, 2, \dots, n$ , and  $P_k = P_{ki}, i = 1, 2, \dots, m$ . For each  $S_k$ , the Voronoi polygon of the laser points was constructed. Subsequently, the statistics was computed for each laser points within its Delaunay neighbors as follows.

The difference in elevation of each laser point with its Delaunay neighbors was calculated and the maximum value found. This value is called  $DiffZ_i$  for laser point  $i$ . This maximum value is the difference in elevation between the top of the buildings and the ground. The overall elevation difference will be

$$DiffZ = \frac{1}{K(m+n)} \sum_{k=1}^K \sum_{i=1}^{m+n} DiffZ_i \quad (1)$$

The standard deviation of elevation in Delaunay neighbors of laser point  $i$  is  $STD_i$ . The overall standard deviation of the ground and building point set are  $StdP$  and  $StdOP$ , respectively.

$$StdP = \frac{1}{Km} \sum_{k=1}^K \sum_{i=1}^m STD_i \quad (2)$$

$$StdOP = \frac{1}{Kn} \sum_{k=1}^K \sum_{i=1}^n STD_i \quad (3)$$

### Improved interpolation

To improve the interpolation, it is required to locate the shadow area. These areas are located near a skyscraper and the distance in horizontal plane to their neighbors is larger than normal. The gap in along track and across track of a laser scanner system is  $gap_{along}$  and  $gap_{across}$ , respectively. Triangulation of the laser points and checking of the distance in elevation and horizontal plane of each laser point within its

Delaunay neighbors, the laser point  $i$  located along the boundary of shadow area satisfies the following condition:

$$\begin{cases} \text{DiffZ}_i \geq \text{DiffZ} \\ \text{DiffXY}_i \geq \sqrt{\text{gap}_{\text{along}}^2 + \text{gap}_{\text{across}}^2} \end{cases} \quad (4)$$

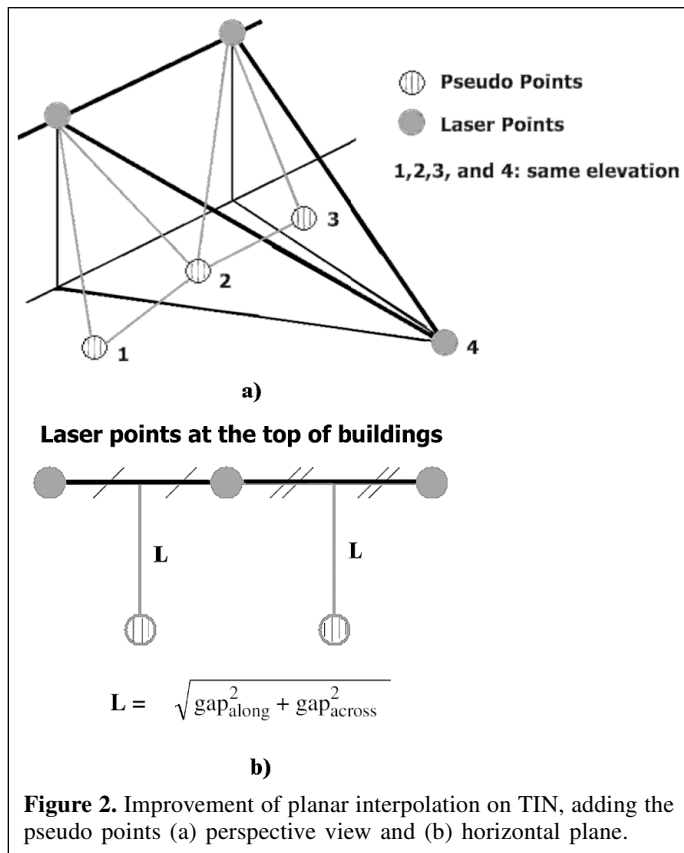
where  $\text{DiffZ}_i$  and  $\text{DiffXY}$  are the maximum of difference in elevation and horizontal plane of laser point  $i$  and its Delaunay neighbors, respectively;  $\text{DiffZ}$  is computed in Equation (1).

For each detected laser points set located along the boundary of the shadow area, the pseudo points can be added as illustrated in **Figure 2a** (in perspective view) and **Figure 2b** (in horizontal plane).

### Wavelet analysis

The mathematical background of the wavelet transform is well presented in many books and articles (e.g., Mallat, 1999). In this study, a discrete wavelet transform was implemented with *à trous* algorithm (Shensa, 1992). To illustrate this algorithm,  $\Phi(x)$  and  $\Psi(x)$  are the scaling and wavelet functions, respectively. The scaling function is chosen to satisfy the dilation equation as follows:

$$\frac{1}{2}\Phi\left(\frac{x}{2}\right) = \sum_u h(u)\Phi(x-u) \quad (5)$$



where  $h$  is a discrete low pass filter associated with scaling function  $\Phi$  and  $u$  is its size.

This equation shows the link between two consecutive resolutions, which differs by a factor of 2, by low pass filtering. The smoothed data  $c_j(k)$  at a given resolution  $j$  and at position  $k$  can be obtained by the method of convolution:

$$c_j(k) = \sum_u h(u)c_{j-1}(k + 2^{j-1}u) \quad (6)$$

The difference between two consecutive resolutions, which is the discrete wavelet transform  $w_j$  (at resolution  $j$ ), was calculated as

$$w_j(k) = c_{j-1}(k) - c_j(k) \quad (7)$$

The wavelet function  $\Psi(x)$  is defined as

$$\frac{1}{2}\Psi\left(\frac{x}{2}\right) = \Phi(x) - \frac{1}{2}\Phi\left(\frac{x}{2}\right) \quad (8)$$

The cubic B-spline with the properties of compact support, symmetry, differentiability, and one zero crossing was chosen to be the scaling function. Because the purpose of the wavelet-based multi-resolution analysis here was to detect the boundaries of the objects based on an object's size, cubic B-spline, which creates the first order of difference information, was the best choice. Therefore,

$$\Phi(x) = \frac{|x-2|^3 - 4|x-1|^3 + 6|x|^3 - 4|x+1|^3 + |x+2|^3}{12} \quad (9)$$

Equation (3) can now be rewritten as

$$c_j(k) = [c_{j-1}(k-2^j) + 4c_{j-1}(k-2^{j-1}) + 6c_{j-1}(k) + 4c_{j-1}(k+2^{j-1}) + c_{j-1}(k+2^j)] / 16 \quad (10)$$

The implementation for 1D data is the convolution with the mask

$$\begin{bmatrix} 1 & 4 & 6 & 4 & 1 \\ 16 & 16 & 16 & 16 & 16 \end{bmatrix}$$

The *à trous* algorithm is easily extensible to the two-dimensional space. This leads to a convolution with a mask of  $5 \times 5$  pixels for the wavelet connected to cubic B-spline scale function. The coefficients of the mask with all elements scaled up to 256 are

$$\begin{bmatrix} 1 & 4 & 6 & 4 & 1 \\ 4 & 16 & 24 & 16 & 4 \\ 6 & 24 & 36 & 24 & 6 \\ 4 & 16 & 24 & 16 & 4 \\ 1 & 4 & 6 & 4 & 1 \end{bmatrix}$$

It is noted that wavelet is one kind of the linear multi-resolution (or multi-scale) analysis. It suffers from the distortion of objects at a coarser resolution. To mitigate the problem, median filter was applied prior to wavelet filtering. The wavelet analysis in terms of pseudo code is therefore outlined as follows:

Input a parameter: the number of the resolutions to be analyzed  
 Init resolution = 1  
 FOR each resolution

- Median filter the original image with the kernel size as  $2^{\text{resolution}} + 1$
- Subtract the median filtered image and the original image to find the difference after median filtering
- Compute the standard deviation, symbolized as  $\sigma$ , of this difference image
- Replace the pixel value of the original image, where the absolute value of the above difference is greater than  $3\sigma$  (i.e., acceptable for most cases), by the value from the median filtered image, thus obtaining the median filtered threshold image
- Convolute this median filtered threshold image with the mask of  $5 \times 5$  pixels as mentioned above for the wavelet *à trous* algorithm with cubic B-spline
- Subtract this smoothed image from one of the previous resolution to obtain the wavelet coefficient image
- Assign the smoothed image to be the original image

End of FOR loop.

A series of wavelet coefficient images across the analyzed resolution was generated. These wavelet coefficient images were used to find the boundaries of the multi-resolution clusters, which depict the existence of objects based on their sizes.

**Cluster boundary detection**

Selection of the appropriate resolutions was made through interactive processing. The decision was dictated by the distribution of the objects in the study area and was operated on two limits. While the lower limit dealt with the finer resolution that appeared at an acceptable level of noise appearance, the upper limit was related to the object’s degree of distortion. This selection reduces the number of resolutions for analysis in the next processing steps to reduce the computational time. It is not a required step and only visual inspection was employed.

From the detailed information of wavelet coefficient images, the chains of the boundaries needed to be generated before converting to vector format for further processing. The starting points were used to lead the tracking pixels of the boundaries. The first criterion for the starting point was that it had only two neighbors in a  $3 \times 3$  local window. The second one was that the combination should not create a sharp angle to guarantee the

continuity of chain. There were 12 types of starting points, listed in **Figure 3**. The construct process could be started with the maps of starting points and the wavelet coefficient images, which presented the cluster boundaries. The direction code in the  $3 \times 3$  local window, which was used to track the direction of the chain, was defined as shown in **Figure 4**.

By tracking the chain in the wavelet coefficient images, the boundaries of the clusters were found across the multi-resolutions space. Subsequently, the detected chain-codes of the cluster boundaries were converted to vector format.

**Checking the laser points at the edges of the clusters**

By a spatial relation of fall-into-boundary, it is possible to distinguish between the qualified object points and the remnants. This processing step is a hybrid method in which the cloud points are grouped and categorized based on the results obtained from the interpolated images. However, there is an ambiguity along the edges of the objects. The classified laser points along the edges of the clusters might fall into the class named fuzzy edge points (which are the overlying object points but classified as the ground points), or the class named wrongly classified points (which are the ground points but classified as the overlying object points). This processing step was employed to clarify these wrongly classified points.

The object point set that has been detected is OP and P is the remainder set of points. The wrongly classified point can be detected by the following equation:

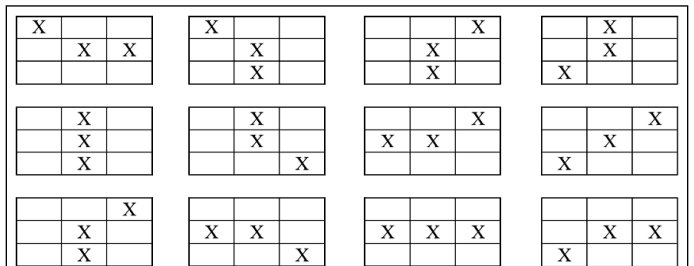


**Figure 3.** Twelve types of starting points for tracking the chain.

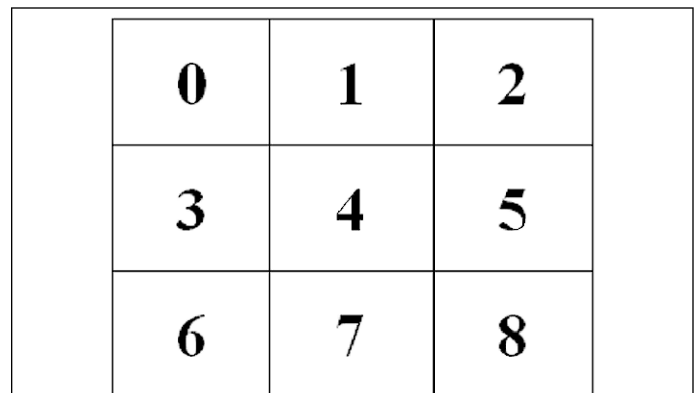


**Figure 4.** Chain code in the local  $3 \times 3$  window.

wrongly classified point set

$$= \left\{ \begin{array}{l} OP_k : (OP_k \setminus \text{in } OP) \text{ and } (P_i \setminus \text{in } P) \text{ and } (OP_k \setminus \text{in } N_i) \\ \text{and } |Z(OP_k) - \text{Ave}Z(N_i)| \leq \text{StdP} \end{array} \right\} \quad (11)$$

where StdP is the given threshold (Equation (2)),  $N_i$  is the Delaunay neighbor point set of ground point  $P_i$ ,  $Z(P_i)$  is the elevation of the point  $P_i$ ,  $\text{Ave}Z(N_i)$  is the average of elevation in  $N_i$ , and  $\setminus \text{in}$  denotes the “is-element-of” symbol.

The fuzzy edge point is a point that satisfies the following condition:

fuzzy edge point set

$$= \left\{ \begin{array}{l} P_i : (P_i \setminus \text{in } P) \text{ and } (OP_k \setminus \text{in } OP) \text{ and } (P_i \setminus \text{in } N_k) \\ \text{and } |Z(P_i) - \text{Ave}Z(N_k)| \leq \text{StdOP} \end{array} \right\} \quad (12)$$

where StdOP is the given threshold (Equation (3)),  $N_k$  is the Delaunay neighbor point set of object point  $OP_k$ ,  $Z(P_i)$  is the elevation of the point  $P_i$ ,  $\text{Ave}Z(N_k)$  is the average of elevation in  $N_k$ , and  $\setminus \text{in}$  denotes the “is-element-of” symbol.

The laser points belonging to the overlying objects, which were detected by the wavelet analysis and have been clarified, were adopted for the calculation of the elevation of the buildings in the following processing steps.

*Processing of the aerial photograph*

The orthorectified aerial photograph was used as the additional data for the detection of the buildings to obtain more information about the shapes of the buildings. Initially, the aerial photograph was co-registered with the interpolated elevation image. Subsequently, this aerial photograph was classified by ISODATA unsupervised classification and local edges detected by the Sobel edge detector. While the boundaries of the clusters from laser scanner data were detected based on size and elevation of objects, the extracted boundaries from aerial photograph were based on the difference in spectral reflectance. The extractable information from aerial photograph is the edges of the classified concrete objects. The quality of this information depends on the specific study area, which is discussed later in this paper.

*Refinement of the detected edges*

The refinement of the detected edges from airborne laser scanner data through the extracted information from the aerial photograph was conducted in a vector format. Firstly, the segments from both scenes, i.e., airborne laser scanner data and aerial photograph, were intersected together to eliminate the redundant information. This redundant information might be as presented in **Table 1**. Secondly, the corresponding segments between two scenes were detected and marked with the same label. The detection was based on the intersection, direction, and the shortest distance between two segments (**Figure 5**). Lastly, the visual refinement was carried out to adjust the

**Table 1.** Redundant information from airborne laser scanner data and aerial photograph.

	Airborne laser scanner data	Aerial photograph
Property	Size is comparable to buildings	Concrete objects
Example	Bushes, trees	Induced by shadow, small concrete objects

mistake in merging the segments as well as checking the closing of the detected boundaries of the buildings.

*Detection of 3D building*

Based on the detected edges from the previous processing, the elevation of a building was obtained by the elevation of the laser points falling within the boundary of the building. The elevation of a building was calculated by the average of all laser points falling within its detected boundary. Subsequently, the attributes of the buildings were imported to build up the 3D database of the buildings and 3D visualization.

**Study area**

Tokyo, located approximately at latitude 35°41'N and longitude 139°41'E, is the most urbanized city in the world with

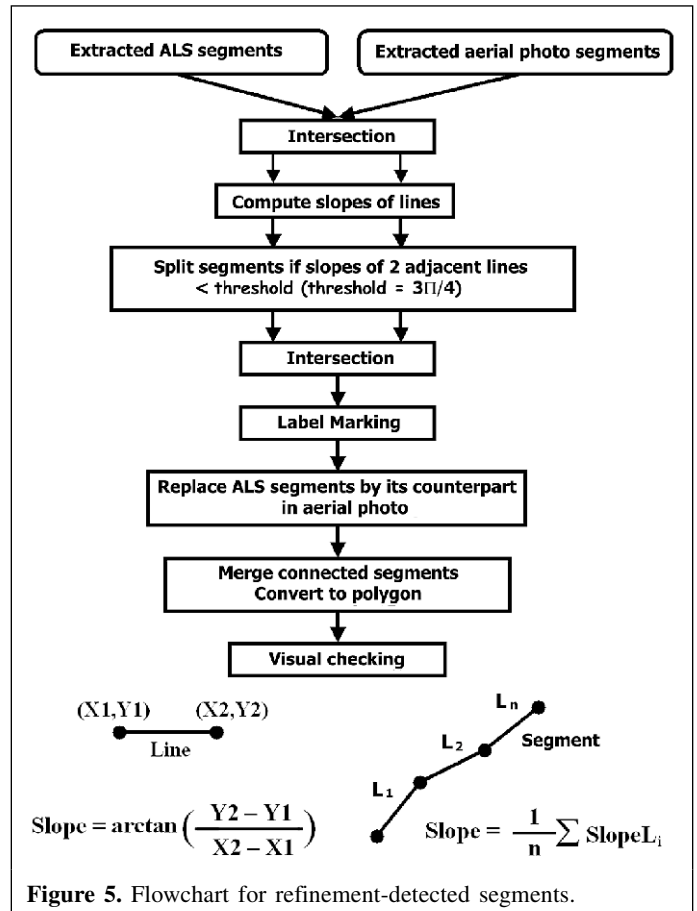


**Figure 5.** Flowchart for refinement-detected segments.

a complex subway system, myriad of housing estates, and office blocks traversed by overhead expressways crowded with traffic. The area of Tokyo is about 2168 km<sup>2</sup> with a population of 12 million. A typical urban area of 512 m × 512 m in Shinjuku-ku, Tokyo, Japan, was selected to test the competence of the proposed algorithm (see **Figure 6**). There are many buildings along with the crowded human activities in this area. The narrow streets appear in the tiny spaces between the very complex structures of the buildings. In addition, there exist numerous moving objects on the streets, and trees aligned along the streets and buildings. Interspersed objects of different sizes typify the study area. Detecting buildings is clearly a challenge.

The parameters of the surveying flight with airborne laser scanner (conducted by Kokusai Kogyo Co., Ltd., Chiyoda-ku, Tokyo) over our testing area is given in **Table 2**. The approximate laser point density of the acquired data is 0.2 points/m<sup>2</sup>. It is quite a low point density for such an application in urban areas. **Table 3** lists the parameters of the aerial photograph that was provided and orthorectified by Nakanihon Air Service (Nakamura-ku, Nagoya City, Japan).

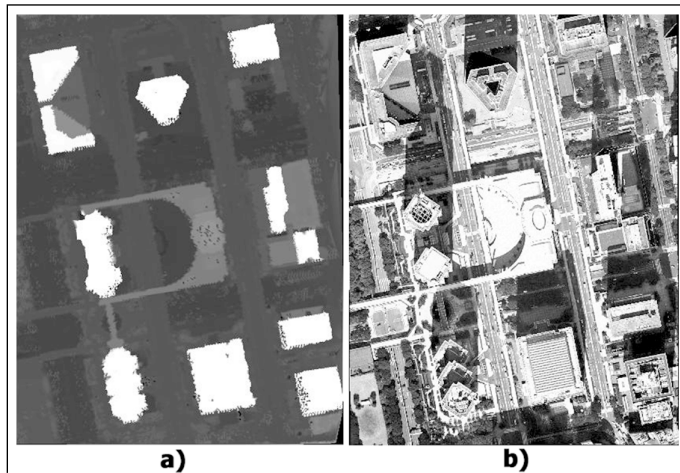


**Figure 6.** Data employed: (a) interpolated image and (b) aerial photograph.

**Table 2.** The parameters of the airborne laser scanner data.

Operation altitude	2700 m
Scan swath width	720 m
Field-of-view	16°
Scan rate	19.5 Hz
Pulse rate	15 kHz
Cross track spacing	1.93 m
Along track spacing	2.83 m
x, y positional accuracy	0.30 m RMSE absolute <sup>a</sup>
z positional accuracy	0.15 m RMSE absolute <sup>a</sup>

<sup>a</sup>RMSE, root mean square error.

## Data processing

### Detection

During pre-processing stage, the orthorectified aerial photograph was co-registered and resampled in the same frame with the laser scanner data. The analysis employed four resolutions. **Figure 7** depicts the smoothed images at two consecutive resolutions by integration of wavelet and median in

**Table 3.** The parameters of the aerial photograph.

Operation altitude	3000 m
Focal length	300 mm
Image size	500 m × 500 m
Image size	2000 × 2000 pixels
Resolution	25 cm × 25 cm
Scale	1:10 000

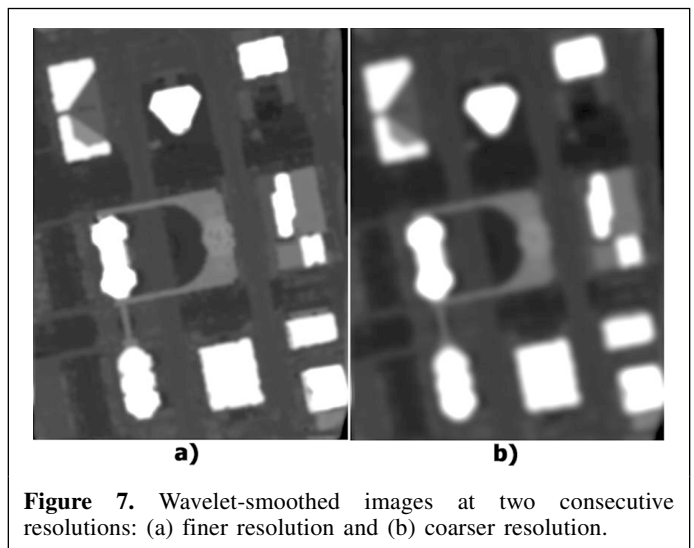


**Figure 7.** Wavelet-smoothed images at two consecutive resolutions: (a) finer resolution and (b) coarser resolution.

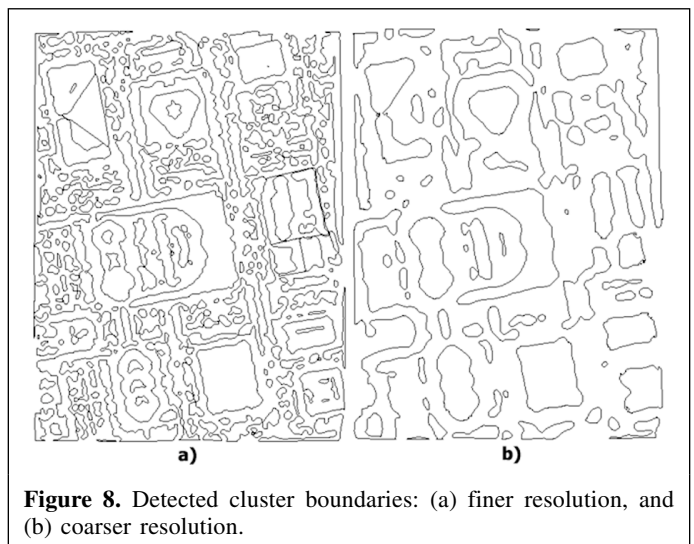


**Figure 8.** Detected cluster boundaries: (a) finer resolution, and (b) coarser resolution.

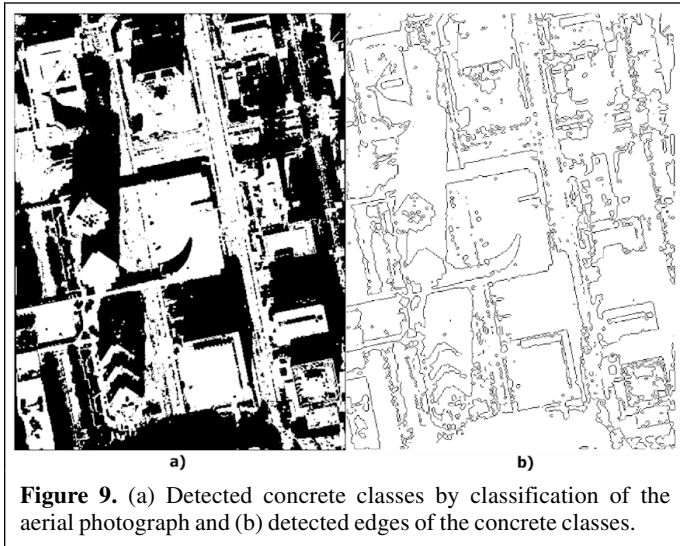


**Figure 9.** (a) Detected concrete classes by classification of the aerial photograph and (b) detected edges of the concrete classes.

multi-resolution analysis. Subsequently, the cluster boundaries were detected and converted in vector format (Figure 8).

The color aerial photograph was employed to assist the construction of 3D buildings through its spectral information. In the study area, there were some classes like concrete, tree, and shadow. However, with the diversity in the spectral reflectance from the concrete, five classes were defined for the running of ISODATA unsupervised classification: vegetation, shadow, concrete1, concrete2, and concrete3. Mathematical morphology, such as erosion and dilation, was applied to eliminate isolated pixels and merge small clusters to the nearby big clusters. Without ground truth data, the unsupervised classification produced an acceptable classified result for visual assessment. Subsequently, the mask was applied to select the concrete classes, which had high probability to be part of buildings (Figure 9a). The result showed many fragments of detected concrete classes owing to the shadows of the skyscrapers. The detected edges of concrete classes are shown

in Figure 9b. Following the scheme described in the previous section, the detected buildings and primary database are shown in Figure 10. Additional data about buildings, such as name of owner, types of services, and number of rooms, can easily be imported into the prepared primary database.

**Accuracy assessment**

The detected buildings were compared with the 2D vector data. Completeness and shape similarity were employed as measurements for accuracy assessment (Henricsson and Baltsavias, 1997). According to the 2D vector data, all buildings in the study area were grouped into nine blocks. The detection completely detected all blocks of buildings (Figure 11). Table 4 shows the results of quantitative evaluation made through shape similarity measurement. The average relative arithmetic difference was 17.71% and the total relative shape dissimilarity was 24.55% in the study area. The difference was induced mainly from the lower parts and along the edges of the buildings such as in the case of building blocks 5 and 8. The problem of missing became worse in the case of block 3 (top right of the scene). In the aerial photograph, the missed buildings showed the spectral information that resembled vegetation. However, in the airborne laser scanner data, they were eliminated in the coarse resolution owing to their small size.

**Visualization**

Another product of this study was the 3D visualization. While Figure 12a illustrates simply the perspective view of the detected buildings, Figure 12b depicts the texture mapping of the detected buildings by the aerial photograph.

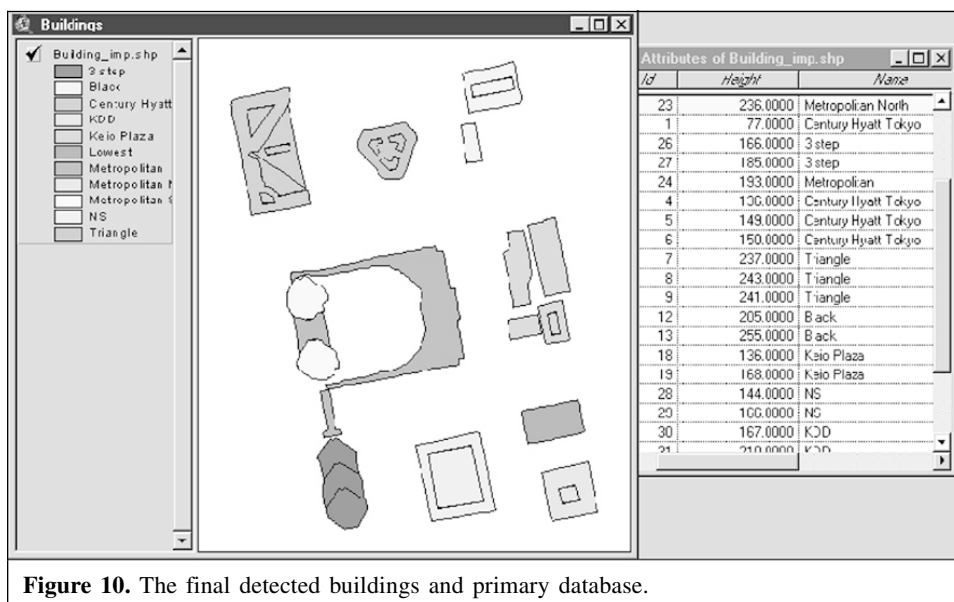


**Figure 10.** The final detected buildings and primary database.

**Table 4.** Accuracy assessment made through shape similarity measurement.

Block	Area (m <sup>2</sup> )		A - B	A/B	B/A	A - B /A (%)	(A/B + B/A)/A (%)
	A	B					
1	8 859.57	8 086.75	772.82	900.99	128.16	8.72	11.61
2	3 687.18	2 762.94	924.24	1024.07	99.82	25.06	30.49
3	5 609.42	3 309.56	2299.86	2399.45	99.59	41.00	44.55
4	11 809.32	11 828.09	18.77	1098.09	1153.95	0.16	19.07
5	10 390.52	6 278.69	4111.84	4308.41	196.57	39.57	43.36
6	3 883.17	3 656.51	226.66	410.75	146.99	5.84	14.36
7	6 488.84	6 070.13	418.70	572.34	153.63	6.45	11.19
8	3 156.35	2 322.82	833.53	1049.10	215.56	26.41	40.07
9	3 046.56	2 856.95	189.61	190.61	1.01	6.22	6.29
Average						17.71	24.55

**Note:** A is 2D vector data and B is detected result.

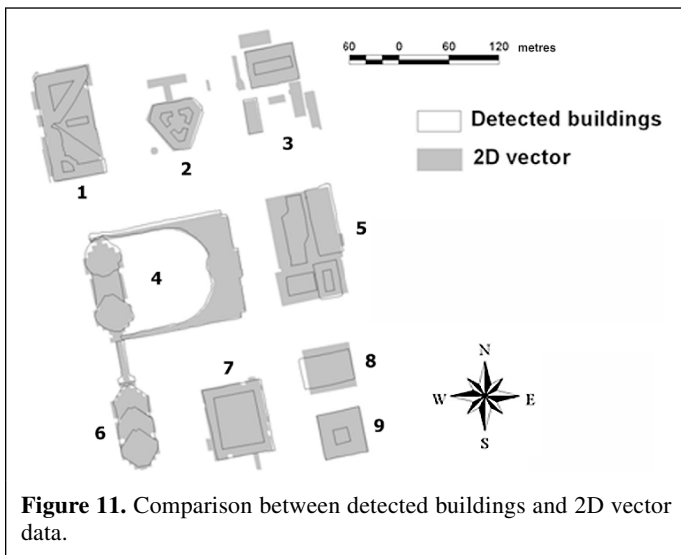


**Figure 11.** Comparison between detected buildings and 2D vector data.

## Conclusion

This study presented an experimental framework based on wavelet analysis to extract buildings from airborne laser scanner data acquired over a dense urban area. This framework is the first stage in developing a processing system for airborne laser scanner data in common usage and is designed to work with various densities of airborne laser scanner data. The low density of laser point data is an obstacle for many applications of laser scanner data in urban areas; the multi-resolution analysis has proved a suitable approach to address this problem. Most buildings in the study area were detected successfully and the results were compared with the 2D vector data. All blocks were detected but the shape similarity did not give good results for some blocks, mainly because of the missing lower parts of the skyscrapers. To obtain higher accuracy in detection, the algorithm was not a fully automatic processing. Further studies are required to improve the level of automation so that larger areas can be processed with higher accuracy and less computation time.

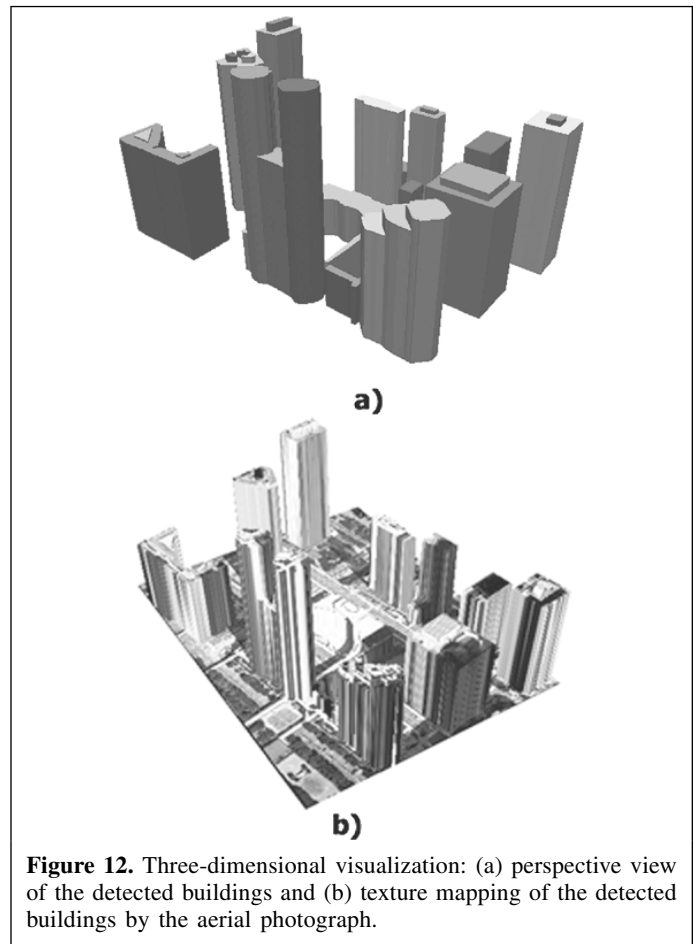


**Figure 12.** Three-dimensional visualization: (a) perspective view of the detected buildings and (b) texture mapping of the detected buildings by the aerial photograph.

## Acknowledgement

Airborne laser scanner data for this study was provided by Kokusai Kogyo Co., Ltd. (Chiyoda-ku, Tokyo, Japan).

## References

- Axelsson, P. 1999. Processing of laser scanner data — algorithms and applications. *ISPRS Journal of Photogrammetry and Remote Sensing*, Vol. 54, pp. 138–147.
- Daubechies, I. 1992. *Ten lectures in Wavelet*. Society for Industrial and Applied Mathematics, Philadelphia, Pa.
- Haala, N. 1994. Detection of buildings by fusion of range and image data. *International Archives of Photogrammetry and Remote Sensing*, Vol. 30, No. 3, pp. 341–346.
- Haala, N., and Brenner, C. 1999. Extraction of buildings and trees in urban environment. *ISPRS Journal of Photogrammetry and Remote Sensing*, Vol. 54, pp. 130–137.
- Henricsson, O., and Baltsavias, E. 1997. 3-D building reconstruction with ARUBA: a qualitative and quantitative evaluation. In *Automatic extraction of man-made objects from aerial and space images (II)*. Edited by A. Grun, E. Baltsavias, and O. Henricsson. Birkhauser Verlag, Basel, Switzerland. pp. 65–76.
- Lega, E., Scholl, H., Alimi, J.M., Bijaoui, A., and Bury, P. 1995. A parallel algorithm for structure detection based on wavelet and segmentation analysis. *Parallel Computing*, Vol. 21, pp. 265–285.
- Maas, H.-G., and Vosselman, G. 1999. Two algorithms for extracting building models from raw laser altimetry data. *ISPRS Journal of Photogrammetry and Remote Sensing*, Vol. 54, pp. 153–163.
- Mallat, S. 1999. *A wavelet tour of signal processing*. Academic Press, London.
- Shensa, M.J. 1992. Discrete wavelet transforms: wedding the à trous and Mallat algorithms. *IEEE Transaction on Signal Processing*, Vol. 40, No. 10, pp. 2464–2482.
- Starck, J.L., and Murtagh, F. 1994. Image restoration with noise suppression using wavelet transform. *Astronomy and Astrophysics*, Vol. 288, pp. 342–348.
- Vosselman, G. 1999. Building reconstruction using planar faces in very high density height data. *International Archives of Photogrammetry and Remote Sensing*, Vol. 32, pp. 87–92.
- Wehr, A., and Lohr, U. 1999. Airborne laser scanning — an introduction and overview. *ISPRS Journal of Photogrammetry and Remote Sensing*, Vol. 54, pp. 68–82.